Pseudo Noise Differential One Way Ranging (PN DOR) Post Processing Overview

Christopher P. Volk,* James S. Border,* and Zaid J. Towfic†

ABSTRACT. — Currently, instrumental phase dispersion is a large error term in the Delta-Differential One-way Ranging (DDOR) error budget. This error arises from the difference in instrumental response to the spectral difference between the narrowband spacecraft signal and the broadband quasar signal. This error term can be reduced in modern transponders by implementing a pseudo-noise (PN) spread spectrum DOR signal instead of the classic sinusoidal DOR signal. This paper presents the methodology to post-process such PN spread spectrum signals and to generate DDOR observables for use in spacecraft navigation. This is now an operational capability in the Deep Space Network (DSN) and is expected to be used for support of CubeSat missions flying with Artemis I and carrying the Iris 2.2 radio.

I. DDOR Background

DDOR is a spacecraft-tracking technique used for deep space navigation. This technique uses Very Long Baseline Interferometry (VLBI) to observe spacecraft and extragalactic radio sources, e.g., quasars, at two stations and to measure the difference in time of signal arrival. During a typical DDOR measurement, an hour-long pass is scheduled concurrently at two (or more) stations. The spacecraft and quasars are observed alternately and recorded using the DSN's Open Loop Receiver (OLR) [1]. Separate channels are used to record frequency slices centered at the received frequencies of the spacecraft tones. The quasar delay measurement is designed to closely match the spacecraft delay measurement so that common mode error cancellation provides high accuracy. The processing of each signal is also designed to have large common mode error cancellation.

The recorded quasar data must first be brought together to a common site for cross-correlation processing [2]. Next, the quasar data from each station are time-aligned and frequency-aligned to find the correlation peak, and then the cross-correlation phase refines the estimate of the difference in signal arrival time. The bandwidth synthesis technique is then used to form a group delay measurement from several discrete frequency channels [3]. The quasar group delay is the phase difference between two channels divided

by the frequency difference between the same channels. Two quasar recordings spanning about 1,000 seconds in time and channels spanning about 40 MHz in frequency, are required to achieve sufficient accuracy.

The spacecraft processing starts by extracting the phase of the spacecraft signal components as a function of time. This is similar to Doppler signal measurements in the DSN, but care is taken to process the signal components in a consistent manner, using coherent models when possible, so that high accuracy is achieved for the phase difference between signal components [4]. This first step can be performed at each station separately or at a central correlator. Next the phase values for each station must be differenced per channel at a central correlator. These channel phase differences are analogous to the quasar processing phase differences and are then used to form group delays in the same manner.

The final output of the DDOR processing system is a group delay for each radio source observation compressed to the center time of the observation. The information content of these measurements is the angular offset between the spacecraft and the quasar. Observables are delivered to the DSN Tracking and Data Delivery Subsystem, where the data are made available and archived in TRK-2-34 format.

This DDOR processing algorithm has roots in the late 1970s. Reference [5] covers the development of DDOR at the Jet Propulsion Laboratory (JPL) from an experimental technique in the 1970s to a key navigation measurement for all Mars landers and many other deep space missions starting in 2001. DDOR is now used to determine the positions of spacecraft and natural bodies with a radio beacon (e.g., Mars with a Mars orbiter) in the International Celestial Reference Frame [6] used for spacecraft navigation. As mission navigation requirements have become more and more stringent, the required accuracy of DDOR measurements has also increased. The processing software has been updated accordingly many times to provide the functionality and high accuracy documented in [1] and [5]. As navigation requirements continue to become more stringent, the technique will continue to require updates.

This paper describes the PN DOR processing algorithm, which was added to the DSN DOR processing software in June 2020. This algorithm presents an opportunity to further improve DDOR accuracy. The PN DOR module was designed to match the interface for the processing of sinusoidal DOR signals. Delay observables for use by navigation are generated from PN DOR signals just as for sinusoidal DOR signals. The DSN now operationally supports PN spread spectrum PN DOR. The first flight with this capability is expected of several of the CubeSat missions flying with Artemis I and using the Iris 2.2 radio [7].

II. PN DOR Motivation and Background

The error budget for a DDOR measurement is based on many factors, including quasar signal level, spanned bandwidth, observation geometry, spacecraft transponder design, ground station receiver performance, and more. The Consultative Committee for Space Data Systems (CCSDS) DDOR Green Book [8] describes these trade-offs in great detail.

Using the current assumptions for an X-band DDOR measurement yields the error budget as shown in Figure 1.

The leading term in this error budget is the instrumental dispersive phase term. This term is the error caused by a difference in the ground station instrumental phase response between the narrowband spacecraft signal and the wideband quasar signal. Currently, the spacecraft signal used in a DDOR measurement has a spectrum with discrete sinusoidal frequency components. The quasar signal, however, is a broadband, white-noise signal. The spacecraft and quasar signal components must be recorded in frequency channels that have the same center frequencies in order to cancel first order instrumental effects. But the channel bandwidths are currently different between the spacecraft and quasar signal. The spacecraft signal is recorded in narrow bandwidths, typically 50 kHz, but each quasar channel must be recorded using a wide channel bandwidth, typically 8 MHz, because the quasar flux ($W/m^2/Hz$) is so low. The dispersive error is caused by the nonlinear instrumental phase effects over the quasar channel bandwidth as compared to the narrowband spacecraft signal. The Instrumental Dispersive Phase error term in Figure 1 of 0.03 ns corresponds to a dispersive phase effect of 0.2° over a 38 MHz spanned bandwidth.

The spectral difference can be greatly reduced by spreading the spacecraft signal with a PN sequence and shaping the spectrum with a shaping pulse. The more closely the spacecraft signal can match the quasar white-noise signal, the more the dispersive phase error is reduced.

Figure 2 shows the X-Band DDOR error budget with the addition of PN spreading overlayed with the baseline error budget from Figure 1. The 90% reduction in dispersive
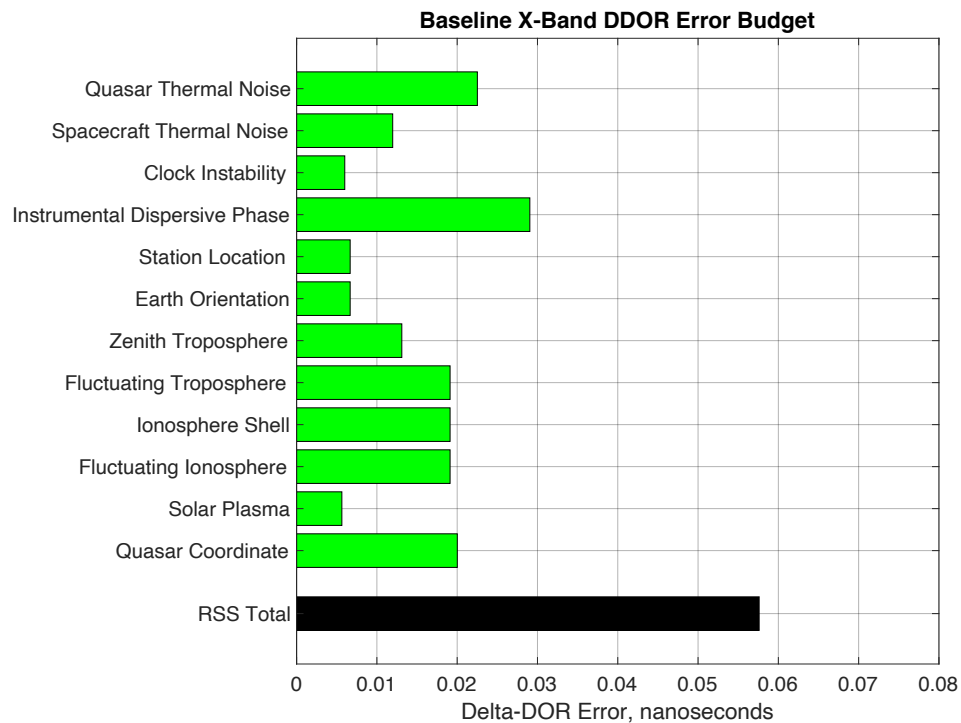

Baseline X-Band DDOR Error Budget

Figure 1. Baseline X-Band DDOR error budget.
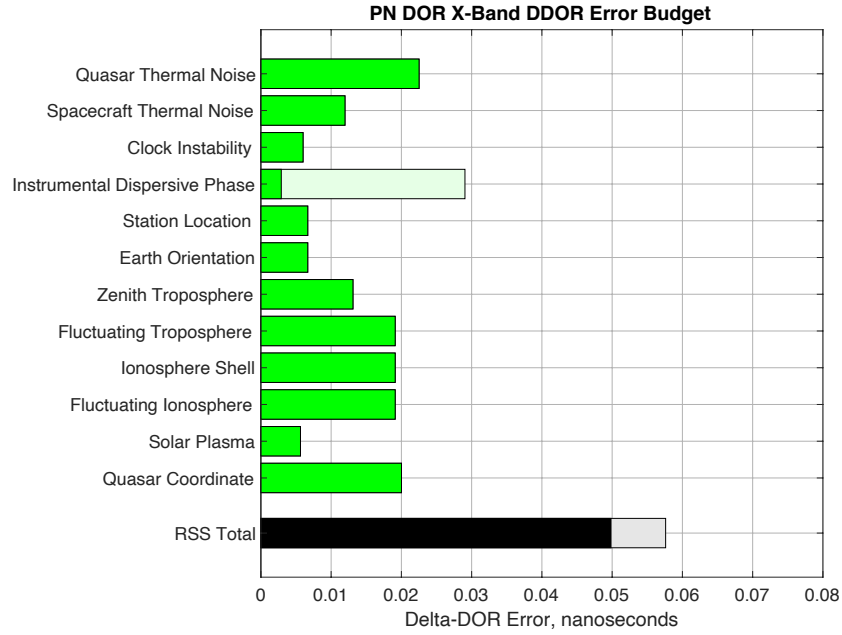
3

PN DOR X-Band DDOR Error Budget

Figure 2. X-Band DDOR error budget with PN spreading (opaque bars) overlaid with the baseline X-Band DDOR error budget (transparent bars).

phase error corresponds to a 15% reduction in root sum square (RSS) error. Under favorable geometric conditions, reduction in the dispersive phase error can result in up to a 40% reduction in RSS error. At Ka-band, charged particle errors are reduced and quasar coordinate errors are expected to be reduced, so the dispersive phase error term could be even more limiting. As more and more missions use Ka-band, PN spreading will become even more critical for high-precision navigation.

The PN spreading on the spacecraft signal is achieved by multiplying the sinusoidal DOR tone with a shaped PN sequence. The CCSDS-recommended PN code for DDOR is a Gold Code, which can be generated with a Linear Feedback Shift Register (LFSR). An example of an LFSR is shown in Figure 3. The feedback taps and the initial seeds can be varied during design, but a common standard is suggested in the CCSDS DDOR Green Book Annex A [8].
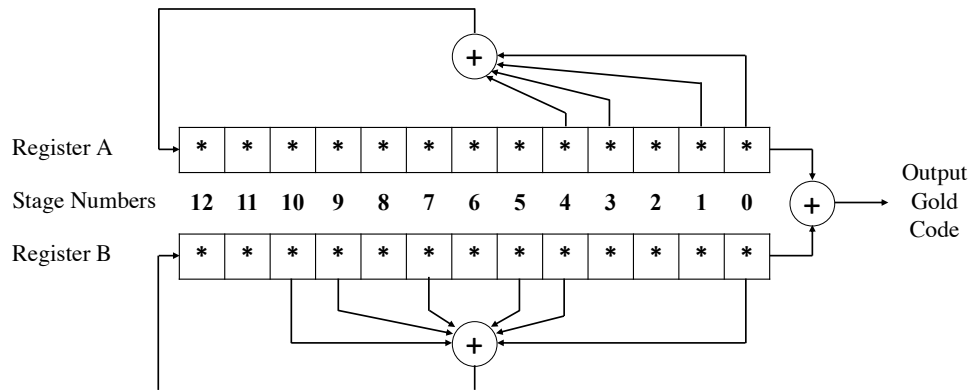

Figure 3. An example Gold Code LFSR. The feedback taps and initial values of the registers are generally programmable to generate different Gold Code sequences.

The output of an LFSR will be a binary sequence. If this sequence is transmitted as a square pulse sequence, then the resulting amplitude spectrum would follow a *sinc(x)* shape. To create a flat quasar-like spectrum, the sequence must be shaped by a shaping filter. The CCSDS DDOR Green Book-recommended shaping filter is a Square Root Raised Cosine (SRRC) Filter. The amplitude spectrum of an SRRC filter at a variety of roll-off factors is shown in Figure 4.
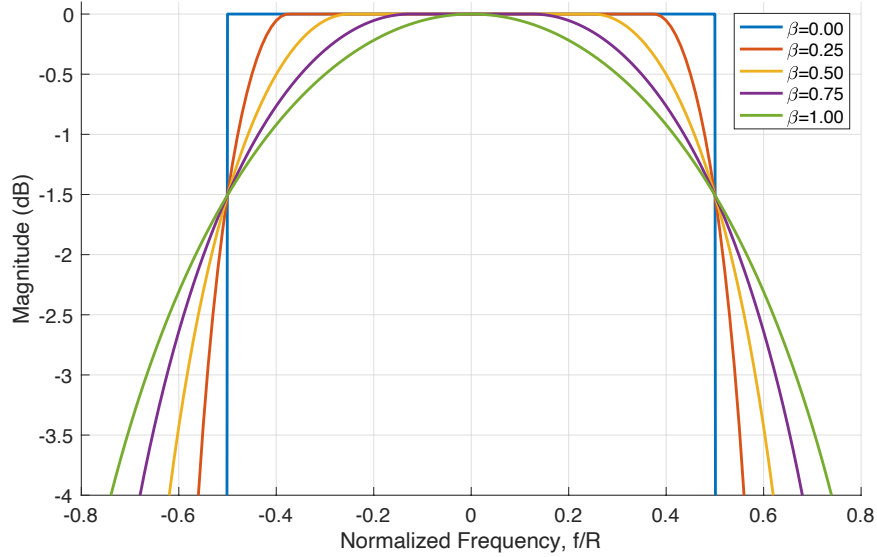

Figure 4. Output spectrum of a square root raised cosine (SRRC) filter. Each different colored line represents a different SRRC roll-off factor, β.

The design of the Gold Code and SRRC Filter are explained in detail in the CCSDS DDOR Green Book Annex A [8]. A prototype design was tested on the Iris transponder engineering model at JPL in 2018. The design was finalized, and PN DOR capability is now operational in the flight model Iris 2.2. Acceptance Testing was successfully completed for Iris 2.2 at the DSN Test Facility, DTF-21, in 2020 [7]. The design process and results for this implementation are described in Reference [9]. The transponder design parameters are needed for successful post-processing and must be documented prior to the pass.

III. PN DOR Post-Processing Overview

The post-processing of a PN DOR signal is similar to conventional DOR signals but with the addition of code that despreads the PN signal. Also different from normal DOR processing is that two phase outputs are generated, one for the underlying DOR tone phase (as in current DOR measurements) and then another for the PN correlation phase. In a PN DOR measurement, the PN phase is used for ambiguity resolution. This post-processing flow is briefly illustrated in Figure 5.
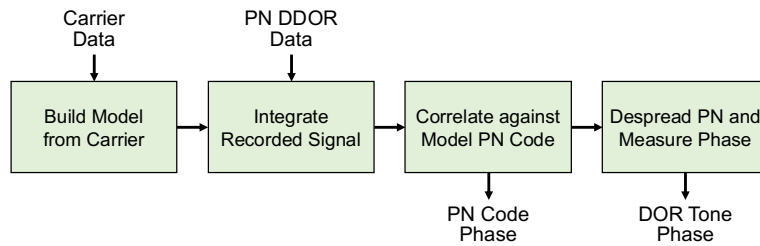
Figure 5. PN DOR Post-Processing Flow Chart.

The following sections describe each step in further detail. One important topic to consider is the runtime performance of the post-processing script. Typically, conventional DOR measurements record the spacecraft data with narrowband (50 kHz) channels, which are very quick to process. For PN DOR, however, the spacecraft data are recorded in much wider channels (similar to quasar signal bandwidths). Special consideration has been added to each step to reduce runtime where possible.

One consequence of using wider channel bandwidths for PN DOR is that the size of the recorded data is much larger than when using narrowband channels. This will cause significantly increased download times if the raw data are sent to a central correlator for processing. This is further exaggerated at Ka-band when 32 MHz channels are used. For example, 30 minutes of spacecraft data (2 PN DOR channels recorded at 32 MHz, 2-bit complex samples) will result in approximately 30 GB of data per antenna. If transmitted at 10 MB/s, it would take approximately 45 minutes to download the data. If instead the data are processed at the antenna first, the output phase time series is less than 30 MB, and the download times are reduced to only a few seconds. Figure 6 shows an example of this procedure.
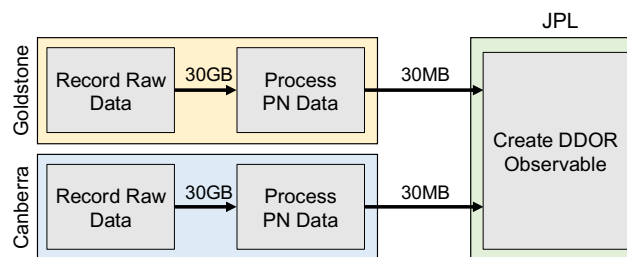

Figure 6. PN DOR processing at each station separately, with the final observable at a central correlator to reduce transmitted file sizes.

A. Step 1: Build Model from Carrier Signal

The first step is to build a PN and DOR phase model from the carrier signal. This assumes that the signals' frequencies are coherent. Under this assumption, the PN Code phase and DOR tone phase are directly related to carrier phase. Because the carrier signal is typically the strongest signal, a high-fidelity model can be built from the carrier phase. This process

is called carrier-rate aiding and is the current process used for most conventional DOR signals.[1]

First, a phase-locked loop (PLL) is run on the carrier signal. The design of such a PLL is left outside the scope of this manuscript. The output of the PLL is the phase of the carrier as measured in the baseband channel. A radio frequency (RF) phase model is needed, however, so the channel center phase must be recorded as well. Typically, this information is found in the headers of the recorded (OLR) data files. Because the channel frequency will be at approximately 8 GHz at X-band (32 GHz at Ka-band), special care is needed to avoid issues with storing large numbers. For example, the down-conversion frequencies are typically common between channels and may cancel to a large extent.

The carrier RF phase can be converted to a model phase for the PN Code and the DOR tone by simply multiplying the carrier phase by a constant multiplier. A common DOR tone multiplier at X-band is 1/440, for example, but decimal numbers can be used as well. This multiplier will vary for each transponder and should be measured before flight. Likewise, the PN Code Multiplier is the multiplier between the carrier phase and the PN code phase. It is important to note, however, that the PN Code Multiplier will convert phase to chips, whereas the DOR Tone Multiplier will yield cycles. In summary, Equations (1) and (2) show how a model can be built from the measured carrier phase.

$$\phi_{DOR}(t) = MULT_{DOR} * \phi_{Carrier}(t) \tag{1}$$

$$\phi_{PN}(t) = MULT_{PN} * \phi_{Carrier}(t) \tag{2}$$

B. Step 2: Integrate Recorded Signal

The model DOR Tone phase can be used now to counter-rotate the raw recorded data to near 0 Hz. This allows for integration over multiple seconds to detect weaker signals. This is performed as in Equation (3), where $V(t)$ are the raw recorded voltage values, and $\hat{V}(t)$ are the counter-rotated voltage values.

$$\hat{V}(t) = V(t)e^{(-2i*\pi*\phi_{DOR})} \tag{3}$$

With the model phase removed, the counter-rotate signal, $\hat{V}(t)$, will contain the PN modulation near 0 Hz. Because the PN sequence repeats the same sequence over and over again, the code can be compressed and averaged into one sequence length. Mathematically, this is equivalent to taking the modulo of the PN phase model in Equation (2) by the code length N_{PN} as shown in Equation (4).

$$\bar{\phi}_{PN}(t) = \left(MULT_{PN} * \phi_{Carrier}(t)\right) \ mod \ N_{PN} \tag{4}$$

The resulting phase will be in the interval (0, N_{PN}). At this point, it is convenient to downsample the data into discrete phase bins for simpler processing in future steps. One

---

[1] When the carrier and the PN DOR signals are not coherent (or when the carrier is fully suppressed), it is possible to utilize a Costas loop to recover the phase of the PN DOR signal directly. However, this technique is not explored in this manuscript.

method for this operation is to bin the data into phase bins and average the complex values into one datapoint per bin. For example, average all of the data points with phase between 0.00 and 0.25 chips into one value. This will greatly reduce the amount of processing for future steps. For example, an 8 MHz file integrated for 2 seconds will have 16 million complex numbers to process, but when reduced to a code length of 8,191 chips (as recommended for X-band) and with 4 bins per chip, there will be only approximately 32,800 complex numbers to process. The number of bins can be varied as desired but must be at least two per chip to satisfy the Nyquist theorem. Because the raw data are averaged per bin, the per-bin signal-to-noise ratio (SNR) is greatly increased during this process while the overall SNR remains approximately unchanged. Figure 7 shows an example of how the raw datapoints may be compressed in this manner. Initially, from the raw data no discernible PN sequence is apparent, but after binning the data, the waveform becomes more apparent.

Note that for the following examples, the recorded I/Q voltage samples (i.e., In-Phase and Quadrature elements) have been shown on separate charts for illustration. The I (In-Phase) samples are shown on the left, and the Q (Quadrature) samples are shown on the right. In practice, it is convenient to work with complex samples instead of treating the I and Q values separately.
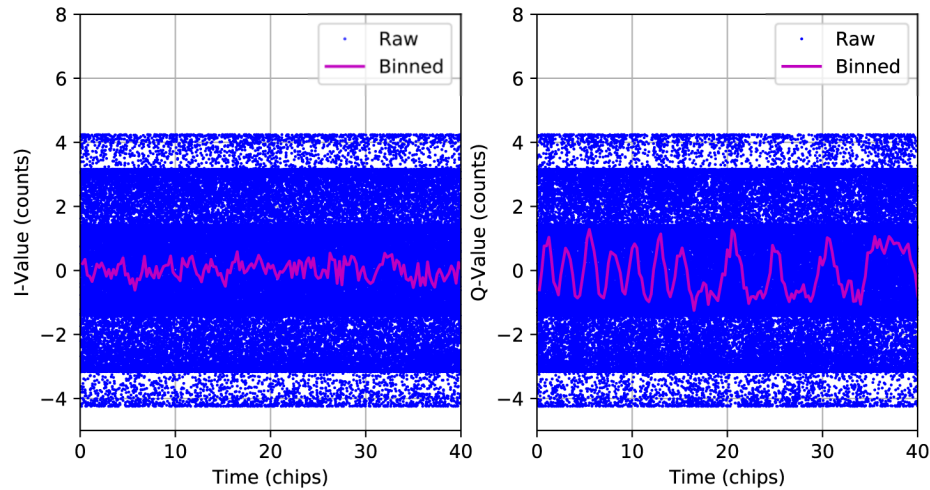

Figure 7. Example of averaging the counter-rotated data (blue dots) into binned data (magenta curve). The In-Phase values are shown on the left chart and the Quadrature values on the right chart.

C. Step 3: Correlate Against the Model Code

The binned data are now ready to be correlated against a reference PN code. This reference code must match the transmitted code and should be created using the circuit shown in Figure 3. The output binary sequence must also be filtered with the same SRRC filter to maximize SNR. One last consideration is that the reference sequence should be binned at the same rate as the binned data. If 4 bins per chip were used previously, then the same should be applied to the reference signal as well.

Figure 8 shows an example of the reference PN signal aligned with the binned data from Figure 7. At this stage in the processing, the difference in amplitude between the In-Phase values and Quadrature values shows the underlying DOR tone phase, which will be measured in Step 4. In Figure 8, the reference PN sequence has been scaled to the same amplitude as the binned values for visual comparison. In practice, both values should be correlated against the same reference PN values with no scaling.
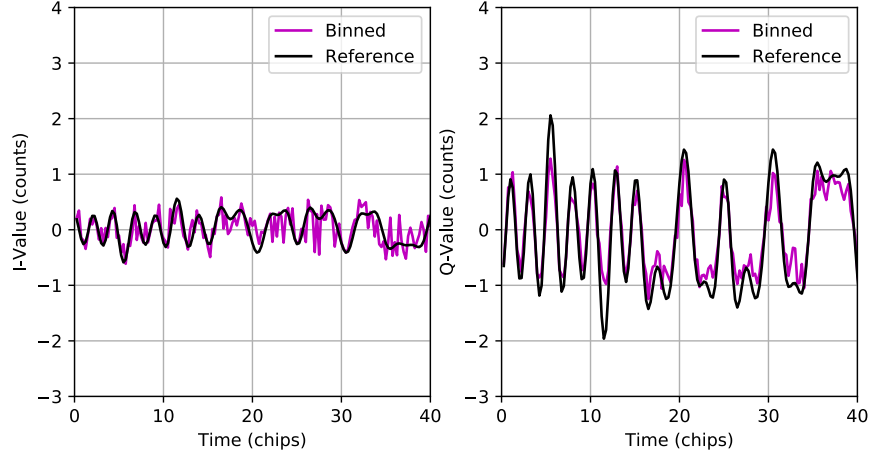

Figure 8. Comparison of the reference PN sequence (black curve) aligned to the binned data (magenta curve). The In-Phase values are shown on the left chart and the Quadrature values on the right chart. The reference PN sequence has been scaled to the same amplitude as the binned data for comparison.

Now, the binned data can be correlated against the reference sequence. This could be done with element-wise correlation, but the processing time can be greatly reduced by using the correlation theorem and fast Fourier transforms (FFTs) as shown in Equation (5). In this equation, $\star$ denotes the correlation operation and $\bar{\mathcal{F}}$ denotes the complex conjugate of the Fourier transform.

$$PN_{measured} \star PN_{reference} = \mathcal{F}^{-1}\left(\overline{\mathcal{F}(PN_{measured})} \cdot \mathcal{F}\left(PN_{reference}\right)\right) \qquad (5)$$

Because element-wise correlation uses $O(N^2)$ number of operations whereas an FTT only uses $O(N \log N)$ operations, there can be a significant improvement for large datasets. Additionally, because the FFT of the reference signal does not change between integration times, the FFT only needs to be computed once for the reference PN sequence instead of at each integration time. Both of these considerations result in a much-reduced runtime when using FFTs instead of element-wise correlation.

The output of the correlation routine will be a series of complex amplitudes versus the number of lags. The lag resolution is related to the downsampling parameter used earlier, e.g., a 4× downsampling factor yields a lag resolution of 0.25 chips. Figure 9 shows an example of the correlation output for all lags.
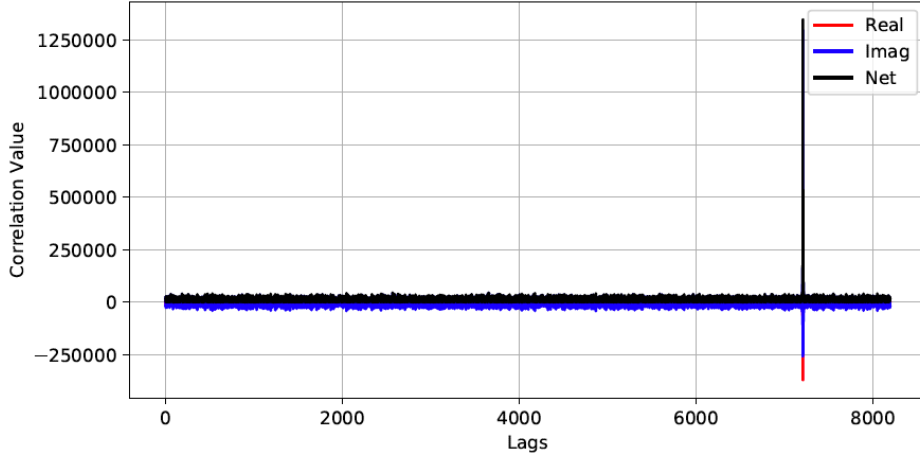
9

Figure 9. Correlation values between the reference PN sequence and the binned data.

The PN DOR code phase can be estimated by finding the peak in the correlation output. To improve precision, it is necessary to interpolate between lags. Quadratic interpolation is suitable for estimating the peak between lags. The DOR tone phase can also be initially estimated from the correlation results by using Equation (6). Here, Q corresponds to the Quadrature-phase value at the peak, and I corresponds to the In-Phase value at the peak. Figure 10 shows a close-up of the peak in this correlation result.

$$\hat{\phi}_{DOR} = \tan^{-1}\left(\frac{Q}{I}\right) \tag{6}$$

The PN correlation SNR, SNR_{PN}, can be computed at this point as well. The SNR_{PN} is computed as the ratio between the peak of the correlation amplitudes and the standard deviation of the correlation amplitudes as shown in Equation (7). This SNR_{PN} provides a measure of how strong the underlying recorded PN signal is and how robust the correlation results are. Monte Carlo analysis shows that for a SNR_{PN} greater than 7.0 dB, the correct PN chip phase can be successfully identified at least 99% of the time.
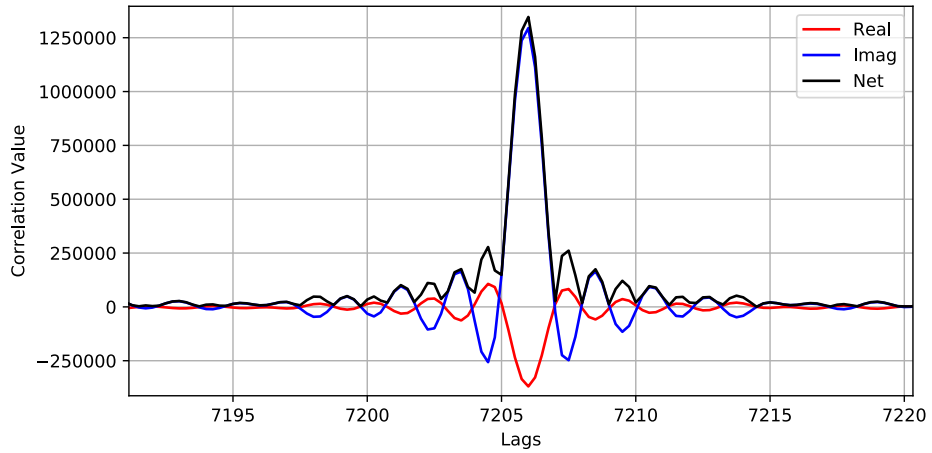

Figure 10. Correlation values near the peak between the reference PN sequence and the binned data.

$$SNR_{PN} = 10 \, log_{10} \left(\frac{max(Amp)}{std(Amp)} \right) \tag{7}$$

Another consideration is that the standard deviation of the PN correlation amplitudes has a lower bound based on the cross-correlation properties of the underlying PN sequence. This creates an upper bound on SNR_{PN}. The cross-correlation properties for Gold Codes (which are recommended for PN DOR) are given in Equation (8), where N is the number of bits in the Gold Code generator circuit.

$$std(Amp) \geq \begin{cases} 2^{(N+1)/2} & for \ N \ odd \\ 2^{(N+2)/2} & for \ N \ even \end{cases} \tag{8}$$

The corresponding upper bound on SNR_{PN} is simply the code length, equal to $max(Amp)$ with no added noise, divided by $std(Amp)$ from Equation (8). A few maximum values for SNR_{PN} are tabulated in Table 1.

Table 1. Maximum SNR for a Variety of Gold Code Lengths.

N (bits)	Code Length (chips)	Max SNR_{PN} (dB)
11	2047	15.049
12	4095	15.050
13	8191	18.061
14	16383	18.062
15	32767	21.072

D. Step 4: Despread PN and Measure Phase

With the PN code phase and DOR tone phase estimated from the PN correlation, the recorded signal can now be despread. First, the binned signal from Figure 8 is counter-rotated by the initial estimated DOR tone phase from Equation (6). This places all of the PN signal on the I-axis and only noise on the Q-axis. This is shown in Figure 11. The reference PN signal is also shown for comparison.
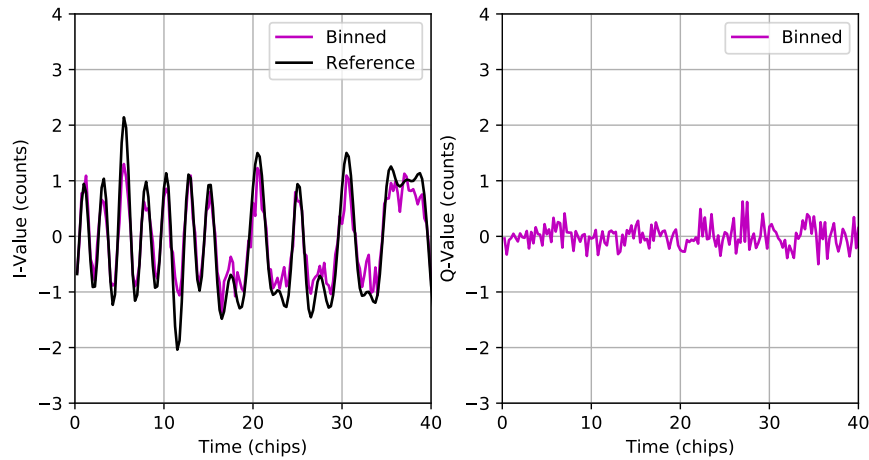

Figure 11. The counter-rotated binned data (magenta curve) places the signal onto the In-Phase axis (left chart) so that only noise remains on the Quadrature axis (right chart). The reference PN signal (black curve) is shown for comparison.

Next, this counter-rotated signal can be multiplied by the reference PN signal to despread the signal. Mathematically, this is achieved by multiplying the binned and reference signals at each time from Figure 11. The result of this multiplication is a despread signal with a direct current (DC) component and high frequency terms. The phase of the DC component is used to refine the DOR tone phase previously estimated during the PN correlation. An example of the resulting despread signal is shown in Figure 12.

The phase of the DC component is measured as the arctangent using the average I-value and the average Q-value within an integration time as in Equation (9). This measured DC phase should be near 0 since an earlier counter-rotation was performed, and so the final DOR phase measurement for the channel is the combination of the earlier estimate and this measured DC phase as in Equation (10).

$$\phi_{DC} = \tan^{-1}\left(\frac{Q_{avg}}{I_{avg}}\right) \tag{9}$$

$$\phi_{DOR} = \hat{\phi}_{DOR} + \phi_{DC} \tag{10}$$

The SNR of this measurement can also be estimated as in normal DOR tone observations. The SNR is estimated as the average of the I-values within an integration time divided by the standard deviation of the Q-values within the same integration time, all normalized by number of points as in Equation (11). This formulation assumes that the counter-rotation performed earlier places all of the signal on the I-axis and thus the Q-axis contains only noise. If there is a significant signal left on the Q-axis, then this equation will result in an erroneous SNR.

$$SNR_{DOR} = 10 \, log_{10}\left(\frac{mean(I)}{std(Q)*\sqrt{1/N}}\right) \tag{11}$$

The SNR of the DOR tone is inversely proportional to the standard deviation of the resulting phase measurement. This relationship is shown in Equation (12). This SNR value is the voltage SNR and can be multiplied by 2 to convert to the ratio of received power to
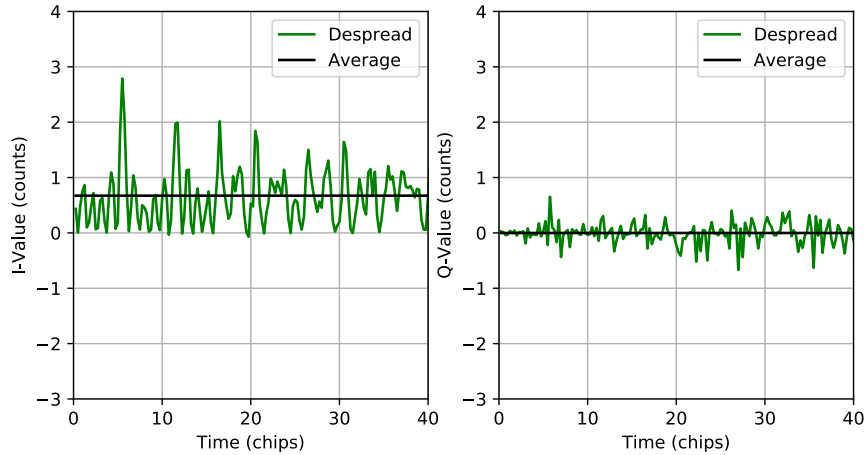

Figure 12. Example of the resulting despread PN data (green curve) and the corresponding average values (black line). The In-Phase values are shown on the left chart and the Quadrature values on the right chart.

noise spectral density, Px/N_0, in dB. The ratio of received power to noise spectral density, Px/N_0, is hereafter, for the sake of convenience, referred to as the received power. The justification for this abbreviation is that Px/N_0 is proportional to the received power when the noise spectral density is constant.

$$\sigma_{\phi,DOR} = \frac{1}{2\pi * SNR_{DOR}}$$

(12)

IV. Performance Assessment

The performance of the algorithm described in the previous section was tested using a Monte Carlo analysis. A software simulator generated data at a specified Px/N_0, and these data were then processed through the PN DOR software. The measured phase was compared to the truth phase to assess the performance of the simulation.

First, data were simulated for a variety of Px/N_0 levels for the recommended X-band configuration (13-bit Gold Code generated at 7.1 Mcps). The results from this assessment are shown in Figure 13. For recording the DOR tone phase, both Classic DOR (sinusoidal tones) and PN DOR yield the same performance, which follows the theoretical relationship shown in Equation (12). The phase sigma on the PN code phase followed a similar relationship but with a constant bias.
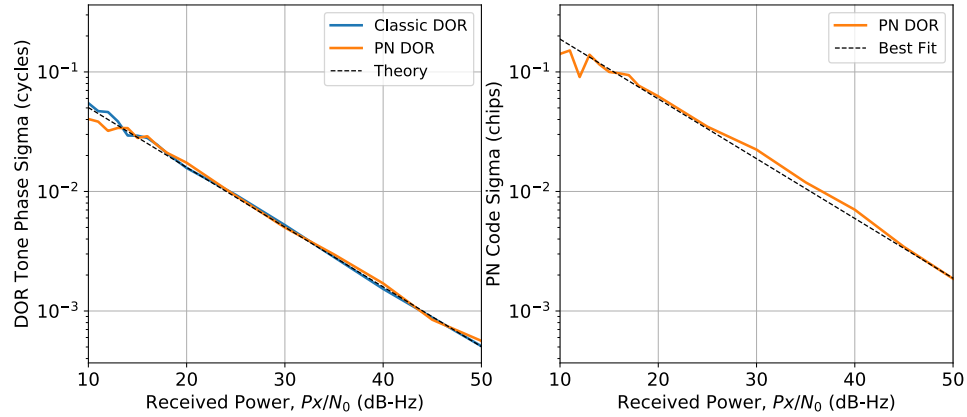

Figure 13. Phase measurement uncertainty for the DOR tone phase (left) and for the PN code phase (right) versus received power. The Classic DOR performance (blue line) is shown for reference against the PN DOR performance (orange line).

The same Monte Carlo analysis was repeated for a few other PN configurations, varying the Gold Code length, chip rate, and in one case, different Gold Code polynomials (denoted as Code 2). Each of these other configurations performed at a similar level as the baseline X-band configuration as shown in the phase sigma results in Figure 14. Although, because the PN code phase performance was the same in terms of PN chips, a higher chip rate results in better time resolution but at the cost of an increased recording sample rate and bandwidth.
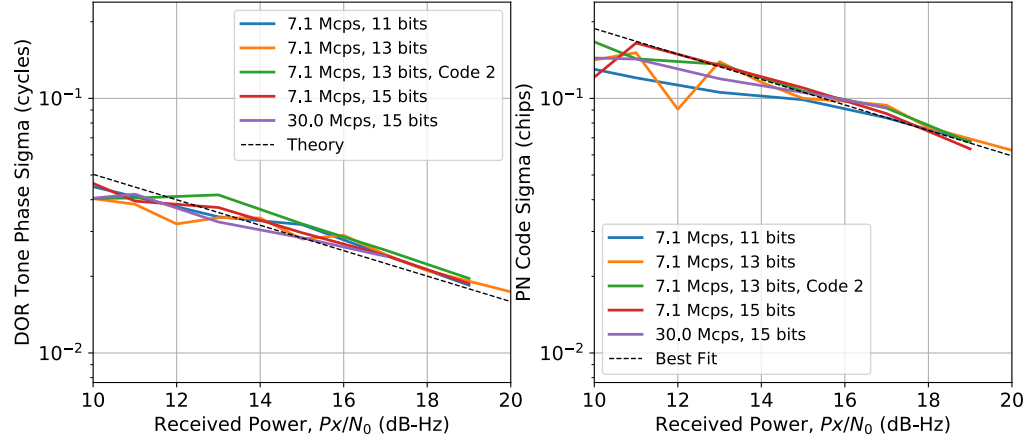
Figure 14. Comparison of DOR tone phase sigma levels (left) and PN code phase sigma levels (right) versus received power for a variety of PN code configurations.

The best fit line plotted on the DOR Tone Phase Sigma (left plot) of Figure 14 is given by Equation (13), which is equivalent to the theoretical relationship in Equation (12).

$$\sigma_{\phi,DOR} = \frac{1}{2\pi*\sqrt{Px/N0}} \tag{13}$$

The best fit line plotted on the PN Code Phase Sigma (right plot) of Figure 14 is given by Equation (14).

$$\sigma_{\phi,PN} = \frac{3.736}{2\pi*\sqrt{Px/N0}} \tag{14}$$

Below a received power of 20 dB-Hz, the probability of successfully detecting the correct PN code phase drops below 100%. This effect is responsible for the noisy behavior visible in Figure 14. The probability of successfully detecting the PN code phase for a variety of code lengths, chip rates, and in one case, a pair of different Gold Code Polynomials (denoted as Code 2), is shown in Figure 15. Shorter PN code lengths increase the probability of detecting the PN code successfully at lower powers but also result in a reduction in ambiguity resolution capabilities. The chip rate or polynomial pair selection does not significantly affect the probability of detecting the PN Code.

Next, a Monte Carlo analysis was performed to assess how the recording sample size impacts the signal level. Typically, DDOR quasar data are recorded with 2-bit samples, so PN data should be recorded at the same sample size to maintain common error cancellation. Other options typically include 1-bit, 4-bit, 8-bit, and 16-bit sample sizes. Table 2 shows how each of these options compare to the 16-bit sampling option. A large decrease in power is observed with 1-bit sampling whereas 4-bit sampling provides almost as much power as 16-bit sampling.
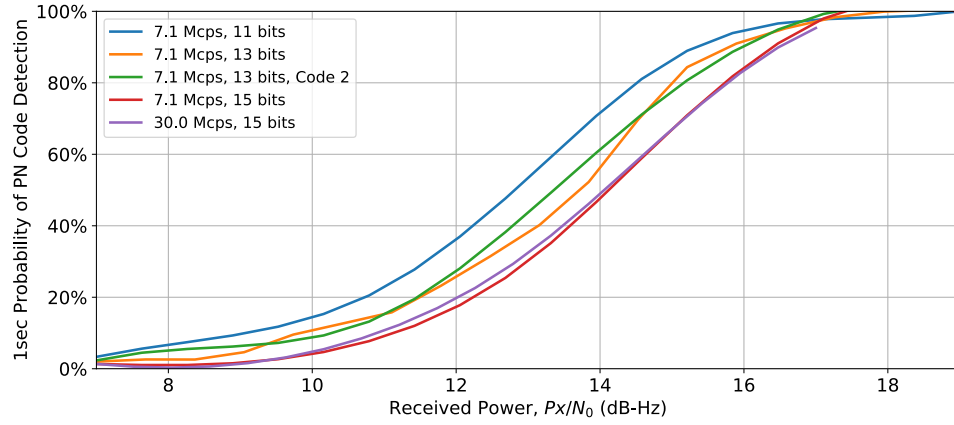
Figure 15. Probability of successfully detecting the PN code versus received power for a variety of PN code configurations.

Table 2. Equivalent reduction in power level for different recording sample sizes.

Sample Size (bits)	Drop in Power Level (dB)
1-bit	−1.92 dB
2-bit	−0.53 dB
4-bit	−0.03 dB
8-bit	−0.02 dB
16-bit	0.00 dB

In summary, the highest performance is achieved with higher chip rates, shorter code lengths, and larger recording sample sizes. This results in the most precise PN Code Phase measurement and highest probability of successfully detecting the PN code. The cost of this configuration is increased data sizes during recording and reduced ambiguity resolution capabilities. Since ambiguity resolution is critical to a successful DOR observable, there is a trade-off that requires moving towards lower chip rates and longer code lengths. For reference, the CCSDS-recommended PN configurations for PN DOR are 13 bits and approximately 7.2 Mcps for X-band, and 15 bits and approximately 28.8 Mcps for Ka-band.

Last, a simulation was created to measure the reduction in phase dispersion error when using PN DOR. In this simulation, an artificial phase dispersion was applied across the 8 MHz channel bandwidth. Five different phase dispersion effects were tested. First was a quadratic effect, and the others were realistic phase dispersion effects as measured by a previous JPL study [10]. The quadratic effect was included as a worst-case estimate because the largest phase dispersions are towards the edges of the bandpass where the PN spreading is weighted the least. Each of the five phase dispersions cases were scaled to produce a phase dispersion error of 0.2° using Classic DOR. The resulting shape for each case is shown in Figure 16, with each case offset by 1° for visual comparison.
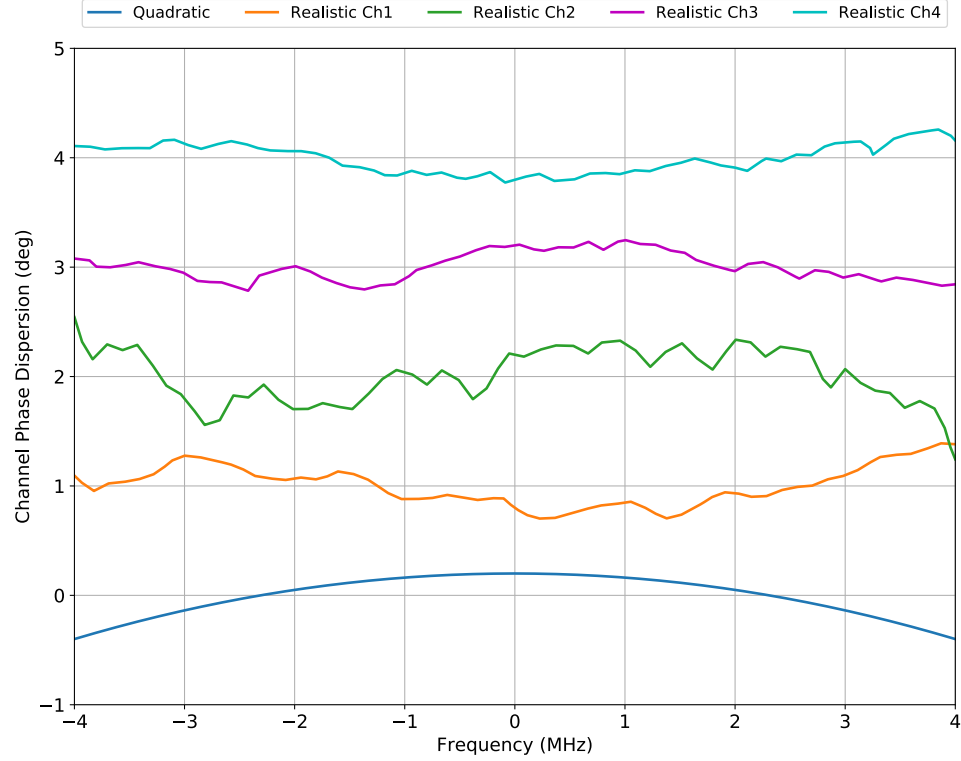
15

Figure 16. Phase dispersion effects tested. Each channel is offset 1° for visual comparison. The realistic channels were measured using quasar data [10] but scaled to yield a 0.2° phase dispersion error.

The spacecraft DOR signal will measure the phase dispersion at the center of the channel, which is 0.2° for all cases. The quasar signal will measure the average phase dispersion across the entire channel bandwidth, which is 0.0° for all cases. The difference between these two measurements is the DDOR phase dispersion error. The PN DOR signal measures the phase dispersion across the channel bandwidth weighted by the shape of the PN DOR spectrum. The PN DOR spectrum shape depends on the shaping filter frequency response, $H(f)$. The CCSDS recommends that a Square Root Raised Cosine filter be used, and the frequency response of such a filer is given in Equation (15). This frequency response depends on the PN Chip rate, R, and the roll-off factor, β.

$$H(f) = \begin{cases} 1 & for & \left(0 \leq |f| \leq \frac{R(1-\beta)}{2}\right) \\ \sqrt{\frac{1}{2}\left\{1 + \sin\left[\frac{\pi}{R\beta}\left(\frac{R}{2} - |f|\right)\right]\right\}} & for & \left(\frac{R(1-\beta)}{2} \leq |f| \leq \frac{R(1+\beta)}{2}\right) \\ 0 & for & \left(|f| > \frac{R(1+\beta)}{2}\right) \end{cases} \qquad (15)$$

The resulting phase dispersion error using a weighted average formulation can be predicted using Equation (16). Because the received signal is filtered once by the transmitter and then correlated against a reference signal that is also filtered once, the resulting phase dispersion error depends on $H(f)^2$. At low roll-off factors (i.e., near 0), the spectrum is flat and nearly all of the phase dispersion is measured, but higher roll-off factors (i.e., near 1) may produce an unsatisfactory reduction in the error.

$$\bar{\phi}_{dispersion} = \frac{\int_{-4\,MHz}^{+4\,MHz} H(f)^2 \phi_{dispersion}(f)\, df}{\int_{-4\,MHz}^{+4\,MHz} H(f)^2\, df} \qquad (16)$$

Data were simulated for each phase dispersion case and for a range of PN chip rates and roll-off factors such that the total spanned bandwidth of the PN signal was equal to the full channel bandwidth of 8 MHz. This condition is satisfied for all combinations where $R(\beta + 1) = 8\,MHz$. The simulated data were processed using the PN DOR algorithm, and the results of the simulations are shown in Figure 17. The theoretical error calculated using Equation (16) is also shown for each case. Note that the Classic DOR phase dispersion error for each case is 0.2° and that at the CCSDS-recommended chip rate (7.2 Mcps), the error is reduced to less than 0.02° for the realistic dispersion curves.
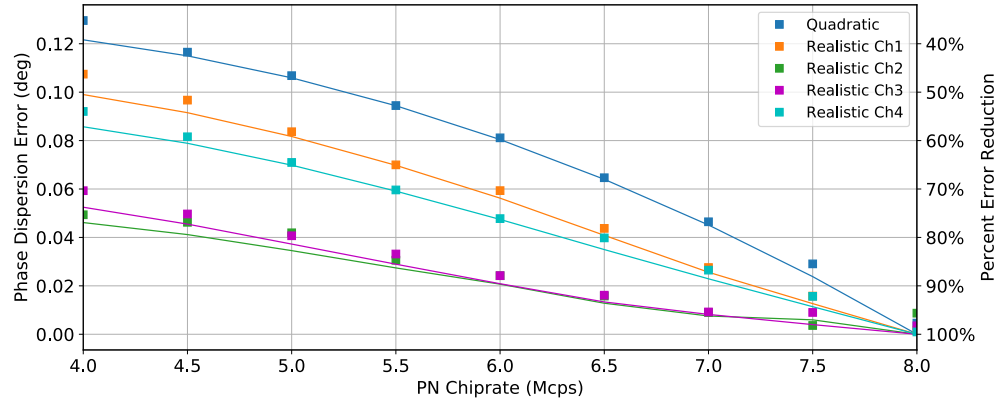

Figure 17. Comparison of the phase dispersion error for each phase dispersion case. The simulated results are shown with markers, and the theoretical values are shown as lines.

In summary, the PN DOR reduction in phase dispersion error varies with the shape of the underlying channel phase dispersion. But in all cases, the error is further reduced at higher chip rates because the PN DOR spectrum is flatter for a greater portion of the channel bandwidth. The CCSDS-recommended parameters for PN DOR specify that the chip rate be at least 90% of the channel bandwidth, and this results in an approximately 90% reduction in the phase dispersion error for realistic phase dispersion assumptions.

V. Summary

As mission navigation requirements become more stringent, increased DDOR accuracy may be required. One novel approach of reducing the DDOR error is the use of spread spectrum PN DOR. This improves common mode error cancellation for the dominant term in the DDOR error budget. PN DOR functionality can be supported in modern digital transponders and has been implemented in Iris 2.2.

References

[1] "Delta differential one-way ranging," DSN Document 810-005, Module 210 Rev. D, Jet Propulsion Laboratory, Pasadena, California, November 2020. https://deepspace.jpl.nasa.gov/dsndocs/810-005/210/210D.pdf

[2] D. D. McCarthy and G. Petit, "IERS Conventions (2003)," IERS Technical Note No. 32. Frankfurt am Main, Germany: Bundesamt für Kartographie und Geodäsie, 2004.

[3] A. E. E. Rogers, "Very long baseline interferometry with large effective bandwidth for phase-delay measurements," *Radio Science,* vol. 5, no. 10, pp. 1239–1247, October 1970.

[4] J. S. Border and M. Paik, "Station delay calibration for ranging measurements," *The Interplanetary Network Progress Report,* vol. 42-177, Jet Propulsion Laboratory, Pasadena, California, pp. 1–14, 15 May 2009. https://ipnpr.jpl.nasa.gov/progress_report/42-177/177C.pdf

[5] B. Bertotti, D. W. Curkendall, and J. S. Border, "Delta-DOR: The one-nanoradian navigation measurement system of the Deep Space Network — history, architecture, and componentry," *The Interplanetary Network Progress Report,* vol. 42-193, Jet Propulsion Laboratory, Pasadena, California, pp. 1–46, 15 May 2013. https://ipnpr.jpl.nasa.gov/progress_report/42-193/193D.pdf

[6] P. Charlot, C. S. Jacobs, et al., "The third realization of the International Celestial Reference Frame by very long baseline interferometry," *Astronomy & Astrophysics,* vol. 644, Article 159, December 2020. doi:10.1051/0004-6361/202038368

[7] "Iris radio v2.2 compatibility test report," DSN Document 872-092-REPORT-200908, Jet Propulsion Laboratory, Pasadena, California, 18 November 2020. Internal Document.

[8] CCSDS 500.1-G-2. "Report concerning space data system standards, delta-DOR technical characteristics and performance," Green Book, Issue 2, November 2019. https://public.ccsds.org/Pubs/500x1g2.pdf

[9] Z. J. Towfic, et al., "Improved signals for differential one-way range," *IEEE Aerospace and Electronic Systems Magazine,* vol. 35, no. 3, pp. 70–79, March 2020.

[10] S. T. Lowe, "A measurement of X-band front-end phase dispersion for delta-differenced one-way range (DDOR) experiments," *The Interplanetary Network Progress Report,* vol. 42-184, Jet Propulsion Laboratory, Pasadena, California, pp. 1–15, 15 February 2011. https://ipnpr.jpl.nasa.gov/progress_report/42-184/184B.pdf